Title

Freezing-modulated-crosslinking: A crosslinking approach for 3D cryoprinting

Authors

Warburton, Linnea
Rubinsky, Boris

Publication Date

2022-08-01

DOI

10.1016/j.bprint.2022.e00225

Freezing-Modulated-Crosslinking: A Crosslinking Approach for 3D Cryoprinting

Linnea Warburton[1], Boris Rubinsky[1,2]

1) Department of Mechanical Engineering, University of California at Berkeley, Berkeley, California 94709, USA

2) Department of Bioengineering, University of California at Berkeley, Berkeley, California 94709, USA

Author to whom correspondence should be addressed: linneawarburton@berkeley.edu

Abstract:

3D Bioprinting is a popular method of fabricating scaffolds for tissue engineering. While soft bioinks such as alginate are useful for reproducing the softest tissues of the human body, it remains difficult to 3D print objects out of bioinks that cannot support their own weight. 3D cryoprinting is a promising method of printing objects out of soft bioinks and creating highly porous scaffolds for tissue engineering. However, crosslinking the frozen objects before they thaw and collapse remains a challenge. Here we investigate a process which we name "freezing-modulated-crosslinking" for crosslinking frozen objects produced by 3D cryoprinting. During freezing-modulated-crosslinking, frozen objects are thawed in a crosslinker bath at a controlled melting rate, so that crosslinking occurs layer by layer and the object can maintain its printed shape. First, we examine the process with a mathematical model to determine the important thermal parameters. Second, we validate our results experimentally by printing a variety of multi-layer alginate objects. By systematically examining this crosslinking approach, we expand the options for 3D cryoprinting. 3D cryoprinted alginate scaffolds can be seeded with cells for use in 3D cell culture or for tissue regeneration.

1. Introduction

3D bioprinting, aka the printing of cell-laden or biologically relevant material, has advanced significantly during the past ten years and is now a widespread manufacturing method for tissue engineering. Many types of 3D bioprinting exist, including laser/light based, inkjet, and extrusion-based, with extrusion-based bioprinting arguably the most widespread method (Ravanbakhsh et al., 2021). Sodium alginate is one of the most popular bioinks used for extrusion-based 3D bioprinting due to its excellent biocompatibility and low cost (Gao et al., 2021, Datta et al., 2019). Previously, alginate-based bionks have been used to fabricate cell-laden scaffolds for the regeneration of bone, cartilage, skin, muscle, neurons, and blood vessels (Gao et al., 2021). Cells can either be mixed with bioink before the 3D printing process or seeded into the scaffold after printing is complete (Dar et al., 2002). The low viscosity of alginate bioinks

makes it easy to extrude through a small nozzle, however, in order for alginate objects to maintain their structure, they must almost always be crosslinked during or after printing. "Crosslinking" refers to the process of forming chemical bonds between polymer chains, making them more rigid. Alginate can be ionically crosslinked, chemically crosslinked, or enzymatically crosslinked among other methods (GhavamiNejad et al., 2020). The timing and rate of crosslinking is a significant challenge for printing alginate bioinks, because if crosslinking occurs before printing, the alginate will be too viscous to extrude through the nozzle, and if crosslinking occurs too long after deposition on the print plate the printed structure will collapse. One approach to printing complicated objects out of soft bioinks such as alginate is to use subfreezing temperatures to solidify/freeze the bioink as it is deposited, a method known as "3D cryoprinting" or "3D cryobioprinting." (Adamkiewicz et al., 2015, Liao et al., 2016, Wang et al., 2017, Tan et al., 2017, Zhang et al., 2019, Ravanbakhsh et al., 2021, Luo et al., 2021)

The advantages of 3D cryoprinting are numerous. First and foremost, 3D cryoprinting can be used to print structures out of soft materials that otherwise could not hold their shape (Tan et al., 2017). Second, ice crystal formation during the freezing process creates highly porous scaffolds, which are ideal for cell adhesion (Luo et al., 2021). Third, freezing cell-laden bionks during printing in a subfreezing temperature support bath can be used to freeze the cells with optimal cooling rates and thereby generate a frozen structure with viable cells. While 3D cryoprinting can be used to build rigid structures out of soft biomaterials, the challenge then becomes transforming these frozen, rigid objects into thawed scaffolds for use in tissue engineering. Many common crosslinking approaches used for 3D bioprinting cannot be used as the object is in a frozen state. Previously, photocrosslinking and internal gelation have been used to crosslink objects fabricated with 3D cryoprinting (Luo et al., 2021, Ravanbakhsh et al., 2021., Remaggi et al., 2022). A drawback of internal crosslinking is that the bioink is only fluid enough to be extruded through the nozzle on the order of minutes before it becomes too viscous to be used. Additionally, reliance on photocrosslinking drastically reduces the number of bioinks that can be 3D cryoprinted as many materials are not photo-crosslinkable. Options for crosslinking 3D cryoprinted objects remain limited, and innovation in this aspect could advance the field.

Previously, we studied the mechanical properties of single-layer cryoprinted alginate in two configurations, a) freezing followed by crosslinking during thawing and b) crosslinking followed by freezing. The mechanical analysis of the products found that the former method yields a material with higher firmness and greater work to shear (Warburton et al., 2022). This paper investigates a method of crosslinking objects fabricated by 3D cryoprinting, which we name "freezing-modulated-crosslinking." This method involves the following steps (See Figure 1). First, during 3D cryoprinting, a low-viscosity alginate bioink is extruded through the nozzle and freezes as it is deposited on the print plate. After printing is complete, the frozen object can be stored in a freezer for short-term or long-term use. Then, when the scaffold is ready to be used, freezing-modulated-crosslinking is used to thaw the frozen object at a controlled rate inside a bath of crosslinker such that it maintains its initial shape. Finally, the scaffold can be used for tissue-engineering applications. For the purpose of this study, freezing-modulated-crosslinking will be investigated as a method of crosslinking frozen, a-cellular scaffolds. For this application, cells can be seeded into the scaffolds after fabrication is complete, similarly to the work of Dar et al. (Dar et al., 2002). The challenge is to control the thawing rate of the frozen object, so that the

rigidity provided by freezing is replaced by cross linking as the Ca+ ions diffuse into the thawed region. This technique is somewhat reminiscent of freeze substitution. Crosslinking alginate structures in a bath of $CaCl_2$ is a common crosslinking technique used in 3D bioprinting. However, to the best of our knowledge, this is the first time that temperature control of the $CaCl_2$ bath has been used to crosslink layer-by-layer in order to maintain the structure of a soft printed object. In addition, this is the first time the parameters of freezing-modulated-crosslinking have been investigated in order to optimize the structure of the printed object.

This paper has two parts, a mathematical analysis and an experimental validation. In the first part, a dimensionless analysis is used to determine what and how the thermal parameters control the process of freezing-modulated-crosslinking. Our mathematical analysis finds that two temperature parameters can be used to control the process: the surface temperature of the melting object and the initial temperature of the frozen sample. In the second part, we qualitatively examine the effect of these parameters by printing various shapes out of 2% sodium alginate and crosslinking them in a $CaCl_2$ bath with freezing-modulated-crosslinking. To further characterize freezing-modulated-crosslinking, we also examine the impact of $CaCl_2$ concentration. The results demonstrate the feasibility of this technique and qualitatively confirms the predictions of the mathematical model. The development of freezing-modulated-crosslinking expands the type of biomaterials that can be used for 3D cryoprinting and the type of structures that can be printed out of soft bioinks.

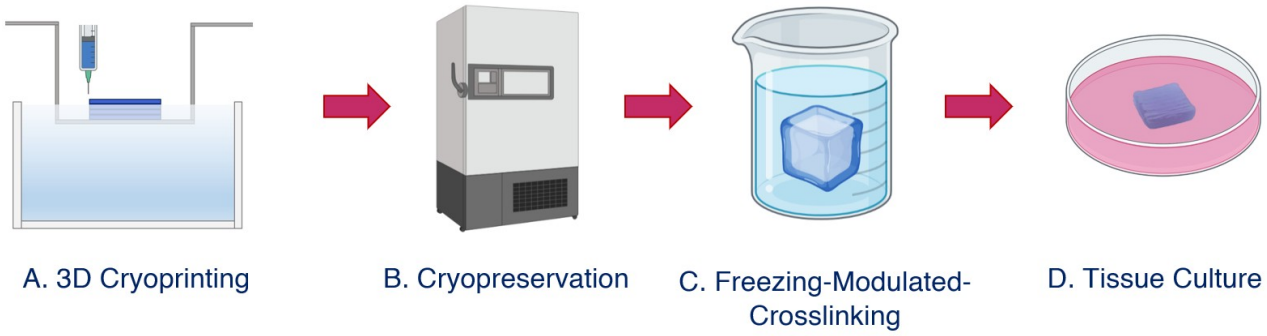

Figure 1. A) 3D Cryoprinting B) The scaffold is kept frozen for either short-term or long-term preservation. C) The object is crosslinked using freezing-modulated-crosslinking. D) The object is ready for tissue culture.

1.1 Freezing-Modulated-Crosslinking

Crosslinking sodium alginate with $CaCl_2$ is simple and cost-effective method of increasing the mechanical strength of alginate bioinks (Hecht et al., 2016). When alginate is in the presence of $CaCl_2$, the Ca^+ ions bind to the guluronate blocks of the alginate chains, and form junctions between guluronate blocks on adjacent alginate chains (Lee and Mooney., 2012). The junctions between the alginate chains create a three-dimensional network, increasing the rigidity of the

polymer (See Figure 2A). During freezing-modulated-crosslinking, the frozen alginate object is immersed in a chilled bath of $CaCl_2$ at a temperature slightly above the melting temperature of alginate. The printed object melts layer by layer, allowing the Ca^+ ions to diffuse into the melted region and crosslink the alginate (See Figure 2B-C). Thus, by controlling the speed of the melting interface on the object it is possible to control the crosslinking interface as well. By melting only a thin layer at a time while the rest of the object remains frozen, the printed object is able to maintain its original shape and prevent collapse. Control of the melting rate is critical to this approach and will be discussed in detail in the mathematical analysis and in the results section.

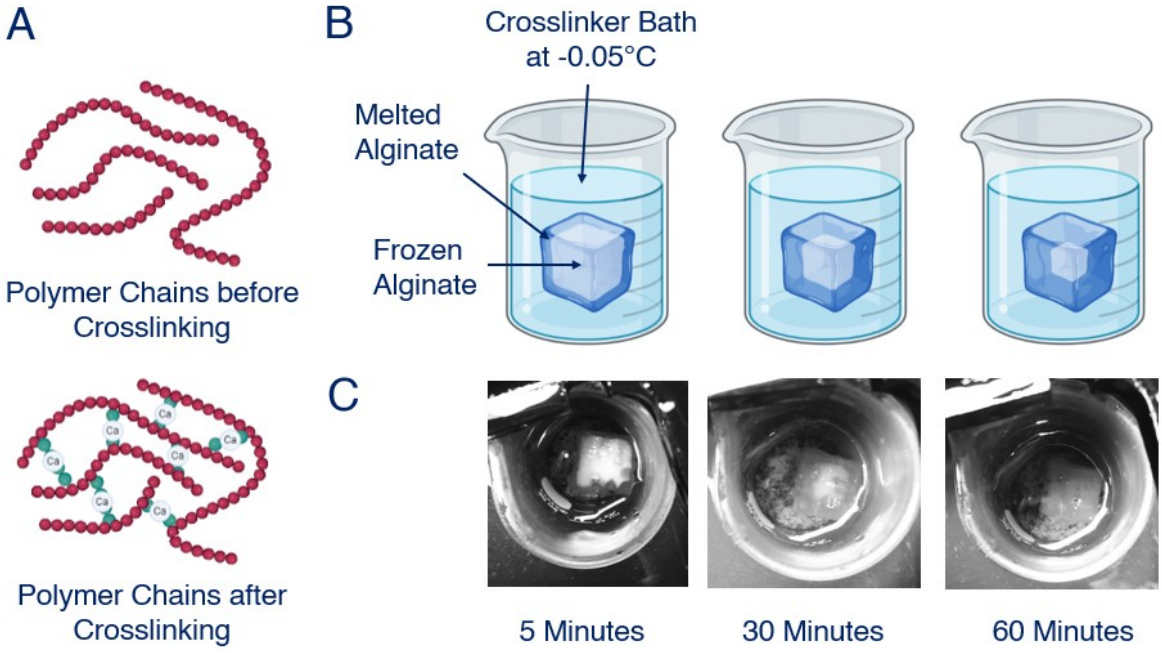

Figure 2. Freezing-Modulated-Crosslinking. A) During crosslinking, Ca^+ ions link alginate chains, creating a 3D network and increasing the rigidity of the polymer. B) Freezing-modulated-crosslinking

2. Mathematical Model

During freezing-modulated-crosslinking, the crosslinker solution melts the frozen object and the Ca^+ ions diffuse into the melted region to crosslink the alginate and provide mechanical integrity. The process is illustrated in the Figure 3 which shows the melting interface propagating into the frozen object, followed by the crosslinking interface. Thermal diffusivity is significantly larger than mass diffusivity. Ideally, the melting interface will precede slightly the crosslinking reaction interface, in such a way that the structural rigidity provided by the ice will be replaced by the crosslinking structural rigidity. The goal of this dimensionless mathematical analysis is to

generate a qualitative understanding about how the different process parameters can be controlled to obtain the design goal.

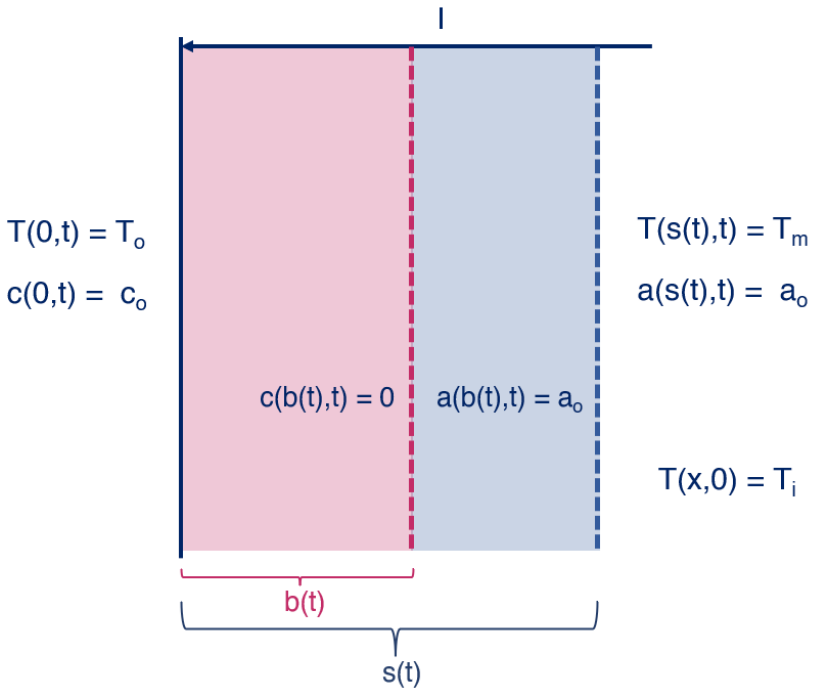

Figure 3. Movement of the melting interface, s(t), and the crosslinking interface, b(t).

In this model, we assume that we analyze the crosslinking of a semi-infinite domain, initially at a temperature T_o, while immersed in a solution of $CaCl_2$ with a calcium concentration of c_o and a temperature of T_o. We also assume good mixing in the solution that surrounds the frozen surface. A similar analysis could be performed with heat and mass transfer convection boundary condition.

Additionally, it is assumed that complete crosslinking occurs at the interface b(t) and that the calcium is completed depleted during crosslinking. The concentration of alginate in the thawed region is assumed to be constant and there is no diffusion of alginate in the crosslinked volume. This assumption is based on reports from experimental studies which state that: "it is evident that the diffusion of free alginate molecules in the gel phase is severely restricted" (Skjak-Braek et al., 1989). It is further assumed that complete melting occurs at the melting interface s(t), which is at the phase transition temperature, T_m. The system is at an initial temperature, $T_i(x,0)$, which is also the temperature far away from the melting interface. The outer surface temperature is, $T_o(0,t)$ and the outer surface concentration of Ca ions is $c_0(0,t)$

The governing equations are the heat and mass transfer equations, and the moving boundaries are defined by conservation of mass at the crosslinking reaction boundary and conservation of energy at the melting boundary.

We dimensionalized the energy equations in the liquid (l) and frozen domains (f) and the mass transfer equation using the following dimensionless variables:

[1]

$$\theta=\frac{T_0-T}{T_0-T_m};\zeta=\frac{x}{l};\tau=\frac{\alpha_l t}{l^2};$$
$$C=\frac{c_0-c}{c_0};A=\frac{a_0-a}{a_0},$$
$$S=\frac{s(t)}{l};B=\frac{b(t)}{l}$$

Where, l, is an arbitrary dimension which could be the desired depth of cross linking or a dimension unit.

The energy equation in the molten region is given by:

$$\frac{\partial\theta_l}{\partial\tau}=\frac{\partial^2\theta_l}{\partial\zeta^2}\,0<\zeta<\frac{s(t)}{l} \quad [2]$$

The energy equation in the frozen region is given by:

$$\frac{\partial\theta_f}{\partial\tau}=\frac{\alpha_f}{\alpha_l}\frac{\partial^2\theta_f}{\partial\zeta^2}\,\zeta>\frac{s(t)}{l} \quad [3]$$

The dimensionless energy equation on the melting interface is given by:

$$\frac{-\partial\theta_l}{\partial\zeta}+\frac{k_f}{k_l}\frac{\partial\theta_f}{\partial\zeta}=\frac{1}{Ste}\frac{dS(\tau)}{d\tau}\,on\,S=\frac{s(t)}{l} \quad [4]$$

Where, α_f, k_f, c_f are the thermal diffusivity, thermal conductivity, and heat capacity in the frozen region respectively and α_l, k_l, c_l are the thermal diffusivity, thermal conductivity and heat capacity in the melted (liquid) region respectively.

The dimensionless initial and boundary conditions are:

[5]

$$\theta_f(\zeta,0)=\frac{T_i-T_o}{T_m-T_o}=V=\theta_f(\infty,t);S(0)=0$$

$$\theta_l(0,t)=0:\theta_l(s(t),t)=\theta_f(s(t),t)=\frac{T_m-T_o}{T_m-T_o}=\theta_m=1:\theta_f(\infty,t)=V$$

Equation [4] shows the emergence of a dimensionless number known as the Stefan number (Ste) which actually governs the behavior of the solution.

$$Ste=\frac{c_l(T_0-T_m)}{L} \qquad [6]$$

Typically, the Stefan number for problems of phase transformation with water, is smaller than 1, which leads to the so-called steady state approximation which will be discussed later.

The dimensionless mass equation for the Ca diffusion problem is:

$$\frac{\partial C}{\partial \tau}=\frac{1}{¿_c}\frac{\partial^2 C}{\partial \zeta^2}\ 0<\zeta<\frac{b(t)}{l} \qquad [7]$$

Where the Lewis number is given by:

$$¿_c=\frac{\alpha_l}{D_c} \qquad [8]$$

The location of the crosslinking interface is found by equating the flux of calcium ions across the crosslinking interface and the kinetics of cross linking, Ψ. The reaction kinetics terms were discussed in many publications, e.g. Kim et al., Mikkelsen et al., Duez J-M et al., and Hajikhani et al (Kim et al., 1990, Mikkelsen et al., 1995, Duez J-M et al., 2000, Hajikhani et al., 2021). According to Kim et al., and Mikkelsen et al., $\Psi=\Psi(\kappa,p,q)$, where κ, is a measure of the reaction kinetics rate, p, is the concentration of the sodium alginate solution and q, is the number of moles of calcium binding per gram of alginate. There are several other ways to define Ψ as in Mikkelsen et al., and Braschler et al. In this study we will assume that Ψ is dependent on the parameters defined by Kim et al., and Mikkelsen et al, which means that it has units of concentration of alginate.

The dimensionless equation on the crosslinking boundary is:

$$\frac{-\partial C}{\partial \zeta}=¿_c\frac{\Psi}{c_0}\frac{dB}{d\tau} \qquad [9]$$

The boundary and initial conditions become:

$$C(0,\tau)=0\, C(B,\tau)=1,\, B(0)=0 \quad [10]$$

The problems to be solved are the energy equations [2], [3], [4] with boundary and initial conditions [5] and the mass transfer equations [7], [9] [15]. These problems are mathematically known as Stefan like problems and examination of the equations and conditions above, leads to the realization that these problems are of the Newman type, which are the only phase transition, chemical reactions problems with a moving interface that have an exact solution. The exact solution and its derivation can be found in Carslaw et al; Ch 11. Since we are interested primarily in the propagation of the mass transfer boundary relative to the heat transfer boundary, we will list here only the solution for the motion of these interfaces.

The propagation of the melting interface is given by Carslaw et al.

$$S(\tau)=2\,\lambda\,¿ \quad \text{or in dimensional form, } s(t)=2\,\lambda\,¿ \quad [11]$$

The value of λ for water and ice was calculated and tabulated (Carslaw et al., 1959). For the dimensionless analysis here, the tabulated data becomes:

V-1 =	0	1	2	3	4	5
$\theta_m=1$	0.056	0.054	0.053	0.051	0.050	0.049

Where $$V-1=\frac{T_m-T_1}{T_0-T_m} \quad [12]$$

V-1 is the ratio between the difference of the initial and the melting temperature and the outer surface temperature and the melting temperature. Obviously the larger the difference the slower is the propagation of the melting interface. This is a design consideration in our technique; to slow down the propagation of the melting interface the larger must be the ratio in equation [12], Note that the case V-1 = 0 is when the initial temperature is the phase transition temperature. This particular case, in which the initial temperature is the melting temperature, and in which the Ste is small, lends itself also to an approximate solution, known as the quasi-steady solution (Rubinsky et al., 1979).

In this case, the energy equation reduces to

$$0=\frac{\partial^2\theta_l}{\partial\zeta^2}\,0<\zeta<\frac{s(t)}{l} \qquad [13]$$

The temperature in the liquid region becomes:

$$\theta_l=(1-\frac{\zeta}{S})\,for\,0<\zeta<S \quad [14]$$

And the solution of the energy equation at the melting interface yields,

$$S=\sqrt{2\,Ste\,\tau} \quad [15]$$

The thermal diffusivity of water at room temperature of $1.4\times10^{-7}m^2/s$and a mass diffusivity of calcium estimate of $1.2\times10^{-9}m^2/s$suggests that the Lewis number for this problem is ¿$(O)=100$. At the time scale when the temperature distribution in the liquid phase is assumed quasi steady, the calcium concentration distribution concentration profile identified by a Lewis number on the order of 100, can be also assumed quasi-steady. It should be emphasized that this assumption was also done by others, e.g. Kim et al.

In the quasi-steady case, the mass transfer equation becomes.

$$\frac{\partial^2 C}{\partial\zeta^2}=0\,0<\zeta<\frac{b(t)}{l} \quad [16]$$

And the solution gives the concentration of calcium ions profile

$$C=(1-\frac{\zeta}{B})\,for\,0<\zeta<B \quad [17]$$

The conservation of mass equation on the crosslinking interface becomes

$$\frac{1}{B}=\Gamma\frac{dB}{d\tau} \quad [18]$$

Where:

$$\Gamma=¿_c\frac{\Psi}{c_0} \quad [19]$$

The solution for the propagation of the dimensionless cross linking interface B becomes very similar in form to the equation for the propagation of the melting interface, with the new dimensionless number Γ, *replacing the* Stefan number (Ste)

$$B=\sqrt{2T\tau} \qquad [20]$$

It should be emphasized that this solution for B is independent on the propagation of melting interface, S.

The goal of this study is to find ways to control the relative distance between the crosslinking interface and the phase transition interface. We have found earlier that the propagation of the phase of change interface can be controlled through the ratio given in [12]. Now, equations [15] and [20] suggest the variable parameters that can be used to affect the distance between the crosslinking interface and the phase transition interface. Interesting the ratio between B and S gives a new dimensionless number that can be used for this purpose.

$$\frac{B}{S}=\sqrt{\frac{\Gamma}{Ste}}=W \qquad [21]$$

This ratio in a dimensional form becomes:

$$\frac{b(t)}{s(t)}=\left\{\frac{\alpha_l \psi L}{D_c c_o[c_l(T_0-T_m)]}\right\}^{1/2} \qquad [22]$$

This equation suggests that decreasing (T_0-T_m), will increase b(t) relative to s(t)

This analysis suggests that it is possible to control the relative propagation of the crosslinking interface to the phase transition interface through control of two thermal terms; (T_0-T_m) and $\frac{T_m-T_1}{T_0-T_m}$

Thus, the goal of the following experimental section is to demonstrate the feasibility of freezing-modulated-crosslinking as a technique and to evaluate how these two thermal terms will affect the outcome of the cryoprinting process.

3. Experimental Validation

3.1 Materials and Methods

3.1.1 The 3D bioprinter

An Ender-5 Plus extrusion-based printer was modified for 3D cryoprinting with the addition of a custom syringe extruder, print plate, and cooling bath (See Figure 4). The cooling bath contained a 45% ethylene-glycol and water solution that was continuously circulated by a Neslab RTE-140 Refrigerated Circulator (Thermo Scientific, Waltham, MA). The solution was circulated from the Neslab RTE-140 through tubes connecting to the cooling bath of the 3D printer, which could then achieve temperatures between -30°C and 23°C, although printing at -15°C yielded the best print results. During printing, biomaterial was extruded through a nozzle onto the print plate, which then descended downward by the height of the printed layer, such that the top layer remained a fixed distance from the cryogenic fluid (See Figure 4B). Thus, the material at the tip of the nozzle was extruded at an identical temperature for each layer. This is notable for two reasons. First, by printing each layer at the same temperature, the printed object is expected to have uniform properties. Second, for cell-laden bioinks, all cells should be kept at specific thermal conditions to maximize cell survival. Currently, the majority of 3D cryoprinters involve printing onto a cooled plate at a static temperature (Liao et al., 2016). A drawback to this approach is that the temperature of the printed material increases as the layers of the printed object grow higher. As a result, the bottom layer of the object is printed under different thermal conditions than the highest layer. The 3D cryoprinter used in this study avoids this issue, as the print plate descends further into the cryogenic fluid after each layer, keeping the temperature at the nozzle fixed.

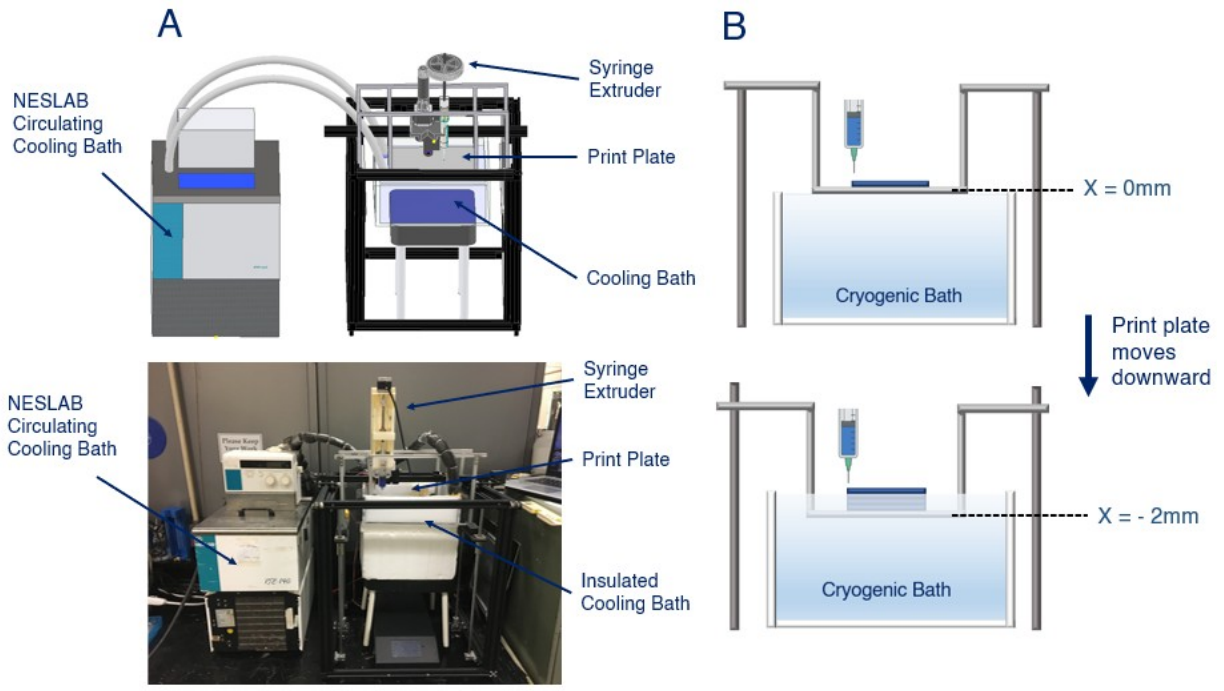

Figure 4. A. The 3D Cryoprinter. B. Printing the first layer of an object. After finishing the layer, the print plate descends further into the cooling bath such that the temperature at the layer being printed is constant.

3.1.2 Printing Parameters

2% sodium alginate was used as the printing ink. The ink was produced by dissolving 2% sodium alginate (Spectrum Chemical Mfg. Corp, Gardena, CA) into de-ionized water. The solution was mixed at room temperature with a magnetic stir plate until it became homogenous and was then stored in a 4C refrigerator for 24h. For photographing the printed objects, blue dye was added to the ink to create increased visual contrast (Watkins, Winona, MN). The abilities of the 3D cryoprinter and freezing-modulated-crosslinking method were demonstrated by 3D printing and crosslinking cubes, rings, and lattices. The bioink was extruded by a custom syringe extruder through an 18-gauge nozzle. The printing speed was 10mm/second, and the temperature of the newly printed layer was fixed at -15°C.

3.1.3 The Crosslinker Bath

Baths of 2%, 4%, or 6% $CaCl_2$ crosslinker were prepared by dissolving 2g, 4g, or 6g of $CaCl_2$ dihydrate powder (Fisher Scientific, Fairlawn, NJ) in 100mL of de-ionized water. A magnetic stir plate was used to mix the solution until it was homogenous. 5% concentration of Pluronic™ F-68 Non-ionic Surfactant was added to the solution to prevent surface forces from distorting the melting interface and thus changing the shape of the printed object (Thermo Scientific, Waltham, MA). The crosslinker solution was then poured into a glass beaker, which was suspended inside the internal cooling bath of the Neslab RTE-140 Refrigerated Circulator (See Figure #D). The internal cooling bath of the Neslab RTE-140 circulated a 45% ethylene-glycol and water solution and could produce temperatures between -45°C and 30°C. The solution was then circulated through tubes that attached to the 3D printer's cooling bath. Based on insights from both the mathematical model and experimental results, the temperature of the crosslinking solution was kept at various temperatures between -4°C and 5°C. Before the frozen alginate object was dropped into the crosslinker, it was kept at either -20°C or -80°C. The optimal temperatures for both the frozen object and the crosslinker bath will be discussed in the results section.

3.1.4 SEM Images

SEM imaging was taken with a Hitachi TM-4000 Scanning Electron Microscope (Hitachi, Tokyo, Japan). The sodium alginate objects were fixed in 2% glutaraldehyde with a 0.1M Sodium cacodylate buffer (pH 7.2). After ethanol dehydration, the objects were dried using a Tousimis Auto-Samdri 815 critical point dryer for one hour (Rockville, MD).

3.1.5 Image Analysis and Statistical Analysis

Images of the 3D cryoprinted lattices were analyzed in ImageJ (NIH, US) to determine the size of the pores. The size of five pores in each of three lattices were analyzed for every set of temperature or concentration parameters. A Student's T-test was used to compare the means with a significance level set at $p < 0.05$. Data points more than two standard deviations from the mean were removed.

3.2 Results and Discussion

3.2.1 Optimizing Thermal Parameters

The mathematical model identified that it is possible to control the propagation of the crosslinking interface by controlling two terms, the initial temperature of the frozen object and the temperature of the crosslinker bath. By varying these two terms, we examined their effect on the outcome of the printed objects undergoing freezing-modulated-crosslinking. The goal of this experiment was to maximize "object accuracy," aka how closely the crosslinked object resembles the intended object in size and shape. Thus, the optimal initial object temperature and crosslinker bath temperature were considered those that produced a crosslinked object which most closely resembled the intended object. 3D cryoprinted lattices were crosslinked under various thermal conditions by varying the object temperature and the temperature of the crosslinker bath (Figure 5.) Based on the Gcode used to print the lattices, the theoretical pore size of a 3D cryoprinted lattice was $1mm^2$. All lattices that underwent freezing-modulated-crosslinking displayed shrinkage. Up to 50% shrinkage is expected for alginate objects crosslinked with $CaCl_2$, (Hazur et al., 2020, Łabowska et al., 2021). However, objects that were melted at faster rates displayed increased shrinkage when compared to those melted at slower rates. The difference in shrinkage between lattices crosslinked at room temperature aka 20°C (Groups A and B) and lattices crosslinked at -0.05°C (Groups C and D) was statistically significant. Therefore, we can conclude that freezing-modulated-crosslinking at an object temperature of -80°C and a crosslinker bath temperature of -0.05°C produces printed objects that most closely resemble the size of the intended objects.

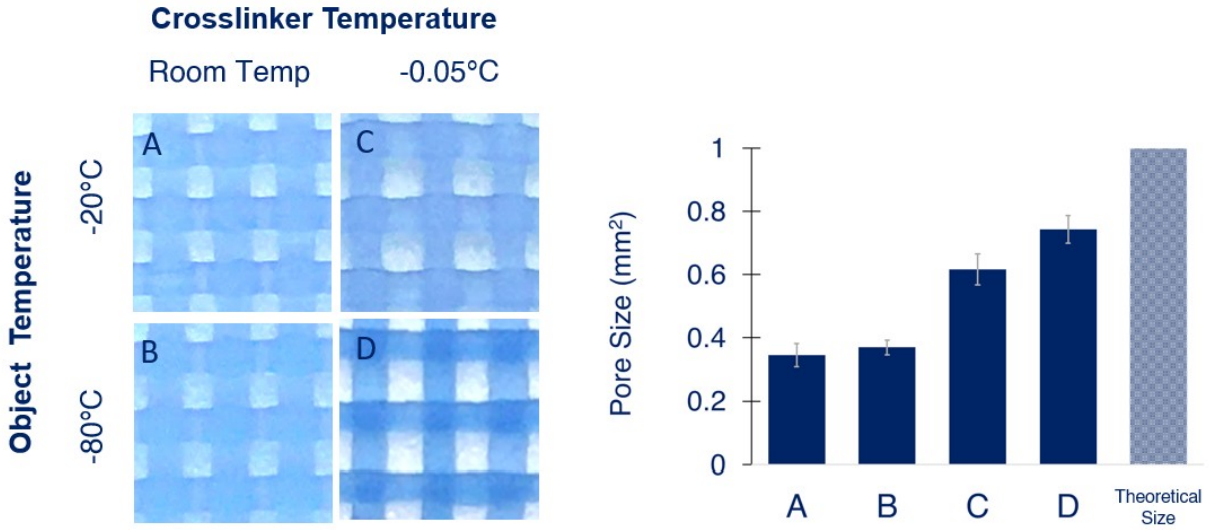

Figure 5. 3D Cryoprinted lattices crosslinked under various thermal conditions. Average pore size was calculated in ImageJ and compiled in the bar graph. Error bars represent +/- one standard deviation from the mean.

In addition to displaying shrinkage, objects crosslinked at faster melting temperatures displayed a "bulging" effect, as shown by the ring in Figure 6A. As stated earlier, the objective of freezing-modulated-crosslinking is to melt the object layer by layer, so that the rigidity of the frozen layer is quickly replaced by rigidity from crosslinking and the object does not change its shape. Based on the mathematical model, we hypothesize that at a faster melting rate the melting interface moves faster than the crosslinking interface, leaving an area of thawed but not yet crosslinked alginate. This soft, thawed area is distorted by the surface tension of the crosslinker bath, creating a "bulged" shape. To counteract the increased effect of surface tension on the printed objects at cold temperatures, a 5% concentration of Pluronic™ F-68 Non-ionic Surfactant was added to the crosslinking solution for each test. Figure 6A demonstrates both the shrinkage effects and the bulging effects that result at faster melting rates. In Figure 6C, objects were allowed to thaw completely before crosslinking, and as a result lost their printed structure completely, demonstrating the need for crosslinking during the melting process rather than after.

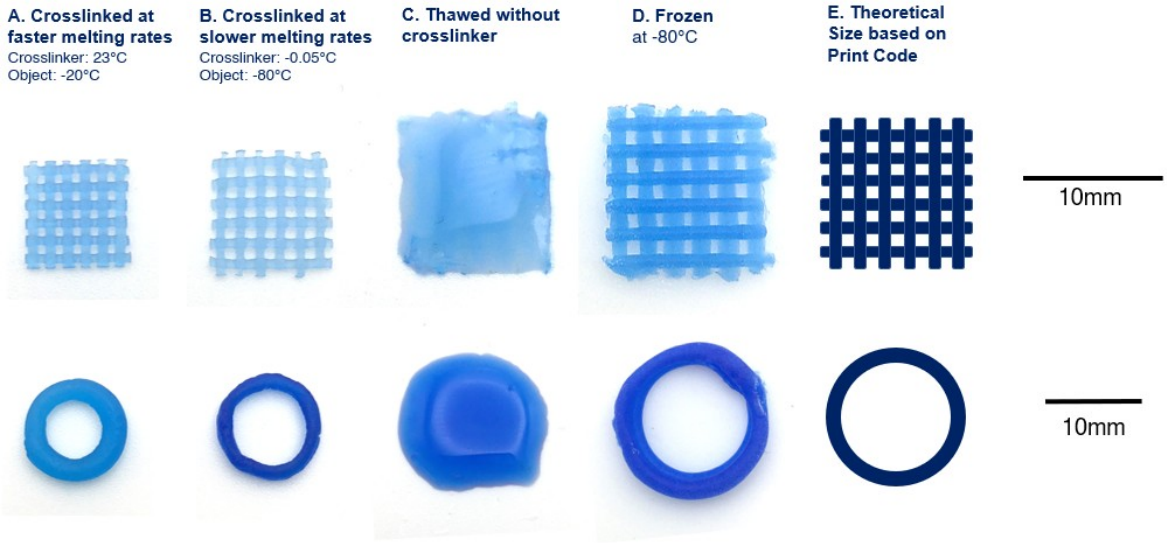

Figure 6. 3D cryoprinted objects crosslinked with various thermal parameters.

As demonstrated by Figure 5 and Figure 6, objects that were crosslinked at a slower melting rate most closely resembled the intended printed object. While using freezing-modulated-crosslinking at even slower melting rates was possible, such as with a crosslinker temperature of -2°C, this increased the crosslinking timeframe and there were no noticeable improvements in object accuracy. Thus, an initial object temperature of -80°C and a crosslinker bath temperature of -0.05°C were considered the recommended parameters for freezing-modulated-crosslinking of alginate objects in $CaCl_2$.

3.2.2 Optimizing $CaCl_2$ Concentration

To further characterize the process of freezing-modulated-crosslinking, objects were crosslinked in various concentrations of $CaCl_2$, including 2%, 4%, and 6%. To quantify the amount of shrinkage, the size of the lattice's pores were measured in ImageJ. Based on the results of the thermal parameter testing, an object temperature of -80°C and a crosslinker bath temperature of -0.05°C were used.

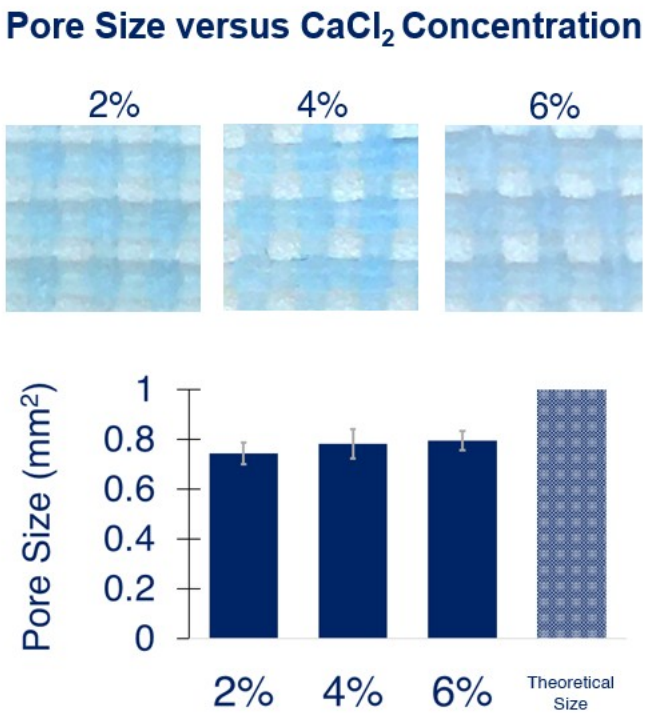

Figure 7. 3D cryoprinted lattices crosslinked in baths with various concentrations of $CaCl_2$. The difference in pore size between concentrations of $CaCl_2$ was not statistically significant. Error bars represent +/- one standard deviation from the mean.

Whether 2%, 4%, or 6% $CaCl_2$ was used in the crosslinker bath, the lattices displayed the same amount of shrinkage. The difference in pore size for lattices crosslinked with different concentrations of $CaCl_2$ was not statistically significant. This result aligns with our prediction from the mathematical model that at slower melting rates the crosslinking interface will propagate more quickly than the melting interface, so that the limiting rate will be that of the melting interface. In this case, the concentration of Ca^+ ions is unlikely to impact the shape of the object as there will not be areas of un-thawed and un-crosslinked alginate that will be distorted by surface tension. Our experimental results suggest that the concentration of $CaCl_2$ does not impact the size or shape of an object crosslinked with freezing-modulated-crosslinking.

3.2.3 Sample Printed Objects

After determining the optimal crosslinker concentration and thermal parameters for freezing-modulated-crosslinking, the applications of this method were demonstrated by 3D cryoprinting and crosslinking various multi-layer objects. (See Figure 8). The following objects were crosslinked at an object temperature of -80°C, a crosslinker bath temperature of -0.05°C, and a $CaCl_2$ concentration of 2%.

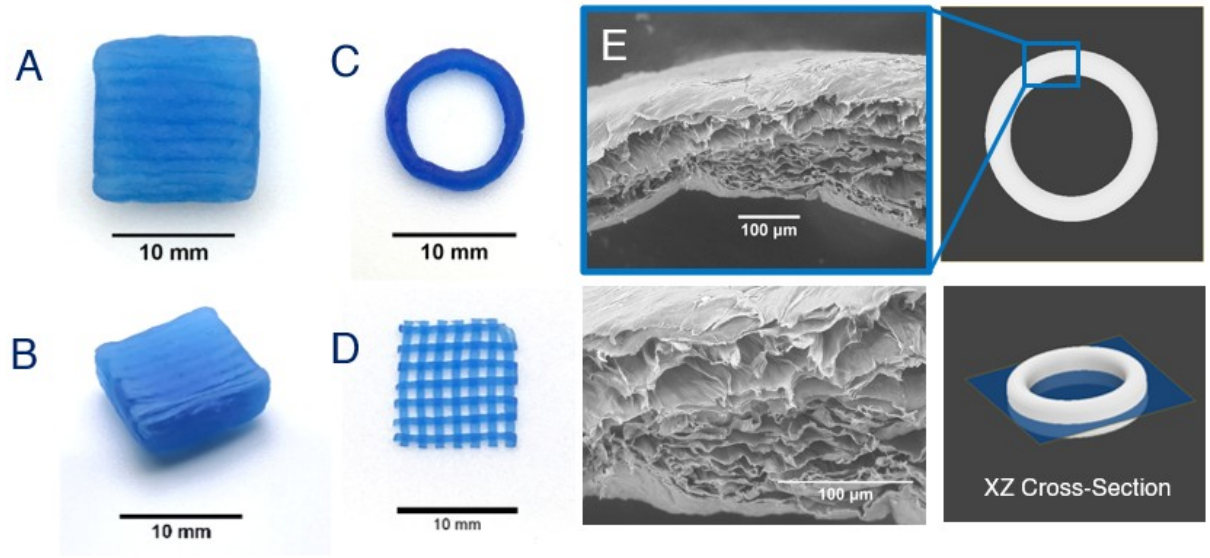

Figure 8. Objects printed with 3D cryoprinting and crosslinked by freezing-modulated-crosslinking. A-B) A 3D cryoprinted Cube. C) A 3D cryoprinted Ring. D. A 3D cryoprinted Lattice. E) SEM images of a 3D cryoprinted ring, obtained with an XZ Cross-section.

Multi-layer objects such as the cube and the ring are difficult to fabricate out of soft bioinks without collapse, as are objects with fine details such as the lattice. To demonstrate the porosity of the scaffolds, SEM images were taken of XZ cross-sections of the 3D cryoprinted rings (See Figure 8E). The SEM images confirmed that 3D cryoprinting creates highly porous objects with directional pores. The pores here are oriented in the Z-direction, as the ice crystals grow upwards from the chilled print plate. Directional pore networks are advantageous for tissue engineering, as they encourage directional cell growth and result in faster diffusion for drug delivery (Feng et al., 2014, Maleki et al., 2019, Tetik et al., 2021). Our previous work demonstrated that by controlling the freezing speed during 3D cryoprinting it is possible control the shape and size of the pores produced in sodium alginate scaffolds (Warburton et al., 2022).

4. Conclusion

This study introduced freezing-modulated-crosslinking as a method of crosslinking 3D cryoprinted objects and used a mathematical model to identify the important thermal parameters. The experimental results demonstrated that this method can be used to crosslink objects printed out of soft bioinks without the objects losing their intended shape. An object temperature of -80°C, and a crosslinker bath temperature of -0.05°C produced objects that most closely resembled the intended results. The concentration of $CaCl_2$ in the crosslinker bath did not have a statistically significant impact on the size or shape of the objects. This examination of freezing-modulated-crosslinking expands the possibilities for crosslinking objects produced by 3D cryoprinting. A limitation of crosslinking alginate bioinks with $CaCl_2$ is that the size of the sample must be small in order for sufficient crosslinker to diffuse through the cryoprinted object. In addition, future studies will need to investigate the impact of the cold temperatures during freezing-modulated-crosslinking on cell viability if this process is to be used with cell-laden bioinks. Future research should also investigate the use of freezing-modulated-crosslinking with other soft bioinks, such as collagen and fibrin.

Acknowledgments

Funding is gratefully acknowledged from the NSF Engineering Research Center for Advanced Technologies for Preservation of Biological Systems (ATP-Bio) NSF EEC #1941543. L.W. was supported by the National Science Foundation Graduate Research Fellowship Program.

Citations

Ravanbakhsh, H., Karamzadeh, V., Bao, G., Mongeau, L., Juncker, D., & Zhang, Y. S. (2021). Emerging Technologies in Multi-Material Bioprinting. Advanced Materials, 33(49), 2104730.

Gao, Q., Kim, B. S., & Gao, G. (2021). Advanced Strategies for 3D Bioprinting of Tissue and Organs Analogs Using Alginate Hydrogel Bioinks. Marine Drugs, 19(12). https://doi.org/10.3390/md19120708

Datta, S., Barua, R., & Das, J. (2019). Importance of Alginate Bioink for 3D Bioprinting in Tissue Engineering and Regenerative Medicine. In (Ed.), Alginates - Recent Uses of This Natural Polymer. IntechOpen. https://doi.org/10.5772/intechopen.90426

Dar, A., Shachar, M., Leor, J., & Cohen, S. (2002). Optimization of cardiac cell seeding and distribution in 3D porous alginate scaffolds. Biotechnology and bioengineering, 80(3), 305-312.

GhavamiNejad, A., Ashammakhi, N., Wu, X. Y., & Khademhosseini, A. (2020). Crosslinking Strategies for 3D Bioprinting of Polymeric Hydrogels. Small, 2002931. https://doi.org/10.1002/smll.202002931

Adamkiewicz, M., & Rubinsky, B. (2015). Cryogenic 3D printing for tissue engineering. Cryobiology. https://doi.org/10.1016/j.cryobiol.2015.10.152

Liao, C.-Y., Wu, W.-J., Hsieh, C.-T., Tseng, C.-S., Dai, N.-T., & Hsu, S. (2016). Design and Development of a Novel Frozen-Form Additive Manufacturing System for Tissue Engineering Applications. 3D Printing and Additive Manufacturing, 3(4), 216–225. https://doi.org/10.1089/3dp.2015.0042

Wang, C., Zhao, Q., & Wang, M. (2017). Cryogenic 3D printing for producing hierarchical porous and rhBMP-2-loaded Ca-P/PLLA nanocomposite scaffolds for bone tissue engineering. Biofabrication, 9(2), 025031. https://doi.org/10.1088/1758-5090/aa71c9

Tan, Z., Parisi, C., Silvio, L. Di, Dini, D., & Forte, A. E. (n.d.). Cryogenic 3D Printing of Super Soft Hydrogels. https://doi.org/10.1038/s41598-017-16668-9

Zhang, Y., Wang, C., Fu, L., Ye, S., Wang, M., & Zhou, Y. (2019). Fabrication and application of novel porous scaffold in situ-loaded graphene oxide and osteogenic peptide by cryogenic 3D printing for repairing critical-sized bone defect. Molecules, 24(9). https://doi.org/10.3390/molecules24091669

Ravanbakhsh, H., Luo, Z., Zhang, X., Maharjan, S., Mirkarimi, H. S., Tang, G., Chávez-Madero, C., Mongeau, L., & Zhang, Y. S. (2021). Freeform cell-laden cryobioprinting for shelf-ready tissue fabrication and storage. Matter, 1–21. https://doi.org/10.1016/j.matt.2021.11.020

Luo, Z., Tang, G., Ravanbakhsh, H., Li, W., Wang, M., Kuang, X., Garciamendez-Mijares, C. E., Lian, L., Yi, S., Liao, J., Xie, M., Guo, J., Zhou, Z., & Zhang, Y. S. (2021). Support Bath-Free Vertical Extrusion Cryo(bio)printing for Anisotropic Tissue Manufacturing. Advanced Materials, 2108931. https://doi.org/10.1002/adma.202108931

Cells, M.-, Remaggi, G., Catanzano, O., Quaglia, F., & Elviri, L. (2022). Alginate Self-Crosslinking Ink for 3D Extrusion-Based Cryoprinting and Application for Epirubicin-HCl Delivery on MCF-7 Cells.

Warburton, L., Lou, L., & Rubinsky, B. (2022). A Modular Three-Dimensional Bioprinter for Printing Porous Scaffolds for Tissue Engineering. Journal of Heat Transfer, 144(3), 031205.

Hecht, H., & Srebnik, S. (2016). Structural Characterization of Sodium Alginate and Calcium Alginate. Biomacromolecules, 17(6), 2160–2167. https://doi.org/10.1021/acs.biomac.6b00378

Lee, K. Y., & Mooney, D. J. (2012). Alginate: Properties and biomedical applications. Progress in Polymer Science (Oxford), 37(1), 106–126. https://doi.org/10.1016/j.progpolymsci.2011.06.003

Skjak-Braek G, Grasdalen H, Smidsrod O (1989) Inhomogeneous Polysaccharide Ionic Gels. Carbohydr Polym 10:31–54.

Kim H-S (1990) A kinetic study on calcium alginate bead formation. Korean J Chem Eng 7(1):1–6.

Mikkelsen A, Elgsaeter A (1995) Density distribution of calcium-induced alginate gels. A numerical study. Biopolymers 36(1):17–41.

Duez J-M, et al. (2000) NMR studies of calcium induced alginate gelation. PartI - MRI tests of gelation models. Magn Reson Chem 38:324–330.

Hajikhani A, Wriggers P, Marino M (2021) Chemo-mechanical modelling of swelling and crosslinking reaction kietics in alginate hydrogels: A novel theory and its numerical implementation. J Mech Phys Solid 153:104476.

Braschler, T., Valero, A., Collela, L., Pataky, K. Brugger, J. Renauld P (2011) Link between alginate reaction front propagation and general reaction diffusion theory. Anal Chem 83:2234–2242.

Carslaw HS, Jaeger JC (1959) Conduction of Heat in Solids (Clarendon Press, Oxford, England, UK). Second Edi.

Rubinsky B, Cravalho EG (1979) The determination of the thermal history in a one-dimensional freezing system by a perturbation method. J Heat Transfer 101(2):326–330.

Hazur, J., Detsch, R., Karakaya, E., Kaschta, J., Teßmar, J., Schneidereit, D., ... & Boccaccini, A. R. (2020). Improving alginate printability for biofabrication: Establishment of a universal and homogeneous pre-crosslinking technique. Biofabrication, 12(4), 045004.

Łabowska, M. B., Jankowska, A. M., Michalak, I., & Detyna, J. (2021). Shrinkage of Alginate Hydrogel Bioinks Potentially Used in 3D Bioprinting Technology. In Key Engineering Materials (Vol. 885, pp. 39-45). Trans Tech Publications Ltd.

Feng, P., Wei, P., Shuai, C., & Peng, S., 2014, “Characterization of Mechanical and Biological Properties of 3-D Scaffolds Reinforced with Zinc Oxide for Bone Tissue Engineering” PLoS ONE, 9(1,

Maleki, H., Shahbazi, M. A., Montes, S., Hosseini, S. H., Eskandari, M. R., Zaunschirm, S., Verwanger, T., Mathur, S., Milow, B., Krammer, B., & Hüsing, N., 2019, “Mechanically Strong Silica-Silk Fibroin Bioaerogel: A Hybrid Scaffold with Ordered Honeycomb Micromorphology and Multiscale Porosity for Bone Regeneration,” ACS Applied Materials and Interfaces, 11(19), 17256–17269.

Tetik, H., Wang, Y., Sun, X., Cao, D., Shah, N., Zhu, H., Qian, F., & Lin, D., 2021, “Additive Manufacturing of 3D Aerogels and Porous Scaffolds: A Review,” Advanced Functional Materials, 2103410, 2103410.